Sixth International Symposium on Turbulence and Shear Flow Phenomena
Seoul, Korea, 22-24 June 2009

DNS AND LES OF CAVITATING TURBULENT FLOW

Kie Okabayashi
Graduate School of Engineering,
Osaka University
2-1 Yamadaoka, Suita, Osaka, 565-0871, Japan
oka-kie@fluid.mech.eng.osaka-u.ac.jp

Takeo Kajishima
Department of Mechanical Engineering,
Osaka University
kajisima@mech.eng.osaka-u.ac.jp

Takashi Ohta
Department of Fiber Amenity Engineering,
Fukui University
3-9-1 Bunkyo, Fukui, Fukui, Japan
t-ohta@mech.eng.u-fukui.ac.jp

ABSTRACT

The two-way interaction between cavitation and turbulence was investigated by the direct numerical simulation of a spatially-developing mixing layer. Namely, the vortical structure and turbulence intensity were compared between single-phase and cavitation conditions. Cavitation mainly occur in the regions of low pressure which are corresponding to vortices. In the braid region, turbulence intensity tends to decrease in comparison with the non-cavitating condition. This decreasing is explained by suppressed energy redistribution by less pressure fluctuation and vortex modification under the cavitating condition. In the fully developed region, on the other hand, collapse of cavity causes velocity fluctuation, so turbulence intensity tends to increase in comparison with single phase flow.

INTRODUCTION

Flows in hydro-machineries are affected by various types of cavitation, and most of them are in turbulence. To simulate cavitating turbulent flows, a variety of methods have been developed. Most of them adopt RANS to deal with turbulence (Coutier-Delgosha, 2003; Kunz, 2000; Senocak, 2002). This method, however, is model-dependent, so it is not useful for understanding of interaction between turbulence and cavitation. Beside, numerical method with RANS is time-averaged, so large-scale unsteadiness in cavitating flow field cannot be considered. On the other hand, LES or DES has become practical tools for unsteady cavitating flows (Ugajin, 2006; Wang, 2007; Wienken, 2006; Yamanishi, 2007). These methods, however, have not taken account of cavitation which occurs in fine-scale elementary vortices, because they are mostly in subgrid scale (SGS). This could reduce the accuracy in predicting turbulent modulation by cavitation as well as cavitation inception (Arndt, 2002). In this situation, we aim at development of cavitation LES model which takes into account cavitation in elementary vortices.

We are going to model the modulation in kinetic energy and dissipation rate of SGS elementary vortices corresponding to cavitation inception or contraction. In this study, we investigate interaction between cavitation and turbulence for LES modeling. We select spatially-developing turbulent mixing layer as the flow field. Mixing layer is a typical free turbulence and there are a lot of theoretical, experimental and numerical investigations for single phase flow. Reducing the cavitation number, interaction between cavitation and typical free turbulence is observed.

OUTLINE OF COMPUTATION

The procedure including cavitation model and numerical method should fit in with the spatio-temporal scale of unsteady motion of vortices in the turbulent shear layer. In this study, we apply the method developed by Okita and Kajishima (2002).

Governing Equation

Hereafter, all variables are non-dimensionalized by a characteristic length H, velocity u_∞, and the liquid density $\rho_{L\infty}$ at sufficiently far position. The flow field is assumed to be isothermal. A low-Mach number assumption (Inagaki, 2000) is applied considering the weak compressibility of liquid.

The governing equations are the conservation laws of mass and momentum of homogeneous mixture of liquid and cavity:

$$\frac{Df_L}{Dt} + f_L\left(M^2\frac{Dp}{Dt} + \frac{\partial u_i}{\partial x_i}\right) = 0 \tag{1}$$

$$\frac{\partial u_i}{\partial t} + u_j\frac{\partial u_i}{\partial x_j} = -\frac{1}{f_L}\frac{\partial p}{\partial x_i} + \frac{1}{Re}\frac{\partial^2 u_i}{\partial x_j \partial x_j} \tag{2}$$

where u_i is the velocity component, p the pressure, and f_L the volumetric fraction of liquid. A Mach number $M(= u_\infty/c,\quad c$ the sound speed) is given uniformly in a computational domain.

Cavitation Model

In the present study, we used following cavitation model

$$\frac{Df_L}{Dt} = \left[C_g(1-f_L) + C_l f_L\right](p - p_v). \tag{3}$$

This model is a modification of Chen's model (Chen, 1995), which is based on the analytic consideration of Rayleigh-Plesset equation. This equation simply means that cavitation region will expand when pressure p is lower than saturated vapor pressure p_v, whereas it will contract when p is higher than p_v. The model constants are $C_g = 100$ and $C_l = 1$. Kajishima et al. (2007) refer some details of derivation of this model.

The saturated vapor pressure p_v is given by

$$\sigma = \frac{p_\infty - p_v}{\frac{1}{2}\rho_L u_\infty^2} \tag{4}$$

corresponding to the cavitation number σ, where p_∞ and $\rho_{L\infty}$ is the pressure and liquid density at far distance.

Numerical Methods

The method of unsteady numerical simulation is based on the fractional step method for incompressible flow. The convective term and viscous term are discretised by central finite difference of 2nd order accuracy. Adams-Bashforth method of 2nd order accuracy is applied for time marching of these terms.

The pressure equation

$$\frac{Df_L}{Dt} + f_L\left\{M^2\left(\frac{\partial p}{\partial t} + u_j\frac{\partial p}{\partial x_j}\right) + \frac{\partial \widetilde{u}_j}{\partial x_j} - \Delta t\frac{\partial}{\partial x_j}\left(\frac{1}{f_L}\frac{\partial p}{\partial x_j}\right)\right\} = 0 \tag{5}$$

where $\widetilde{u_j}$ is fractional step and is derived from equation 1, is discretized using 3-step method for time difference and 2nd order central difference for space. Eq. 5 is converged by the relaxation method. Then using the pressure calculated from above procedure, the velocity at next step is directed by adding the pressure gradient to the fractional step and time marching is completed. Time marching for liquid volumetric fraction f_L is semi-implicit scheme and conducted for two-stage. Readers can find a detail of our numerical method in Okita and Kajishima (2002).

Computational Condition

The flow field is a spatially-developing turbulent mixing layer as shown in Figure 1. The height H is selected for the length scale. The size of the domain is $H_x = 10H$ in the mainstream direction and $H_z = H$ in the spanwise direction. The periodicity is assumed in the spanwise direction. In this computation, velocity ratio U_1/U_2 is 2. The mean velocity difference $\Delta U = U_1 - U_2$ is used for the velocity scale. In a mixing layer, primary roll-cell vortices are generated due to Kelvin-Helmholtz instability. In the stretched region between two neighboring vortices, streamwise (rib) vortices are caused by the secondary instability.

The inflow condition consists of the mean velocity given by a hyperbolic-tangent profile, on which three-dimensional random perturbations are superposed:

$$u(0,y,z,t) = \frac{U_1+U_2}{2} + \frac{U_1-U_2}{2}\tanh\left(\frac{2y}{\delta_\omega}\right) + u'(y,z,t) \tag{6}$$

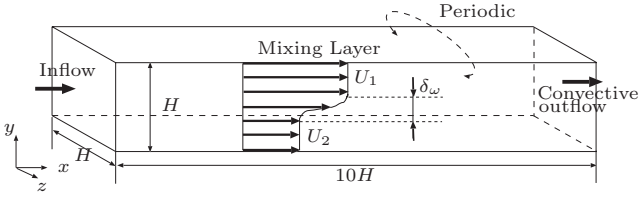

Figure 1: Overview of computational domain and boundary conditions.

Table 1: Parameters for simulation.

grid points	$N_x \times N_y \times N_z$	$384 \times 192 \times 120$
grid size	$\min[\Delta x]$	$0.01071H$
	Δy	$0.00521H$
	Δz	$0.00833H$
Reynolds number	$Re(= H\Delta U/\nu_L)$	1×10^4
Mach number	M	0.1
time increment	Δt	$5 \times 10^{-5} H/\Delta U$
cavitaiton number	σ	$0.5, \infty$ (single phase)

$$v(0,y,z,t) = v'(y,z,t) \tag{7}$$

$$w(0,y,z,t) = w'(y,z,t) \tag{8}$$

Here, the vorticity thickness δ_ω at the inlet is defined as follows:

$$\delta_\omega = \frac{\Delta U}{(\partial U(y)/\partial y)_{\max}} \tag{9}$$

where $U(y)$ is the mean velocity at the inlet. In this computation, δ_ω is set at $0.01H$. The velocity perturbation is given by uniform random numbers, and their amplitude is set at less than 1% of ΔU. At the outflow boundary, convective boundary condition without reflection as described in Okita and Kajishima (2002) is used. In transverse, U_1 is given for the velocity at upper boundary, U_2 at lower boundary. pressure boundary condition is set by Neumann boundary condition at the inflow and transverse boundary, and by Dirichlet condition at the outflow. Other parameters for this computation are shown in table 1. As for computational grid, the spacing of grid points in x-direction is finer near the inflow. In the bottom of table 1, cavitation number σ is set at 0.5 for cavitating condition; ∞ for non-cavitating condition (single phase).

OBSERVATION OF THE FLOW FIELD

A DNS of a turbulent mixing layer in cavitating condition is conducted. In following discussion, 'cavitation inception' region is assumed as the region where liquid volumetric fraction f_L is less than 1. Figure 2 represents the instantaneous profiles of vortical structure and cavity. Figure 2(a) and (b) represent front view and top view of the flow field, respectively. Here, vortical structure is indicated by isosurface of second invariant of velocity gradient tensor Q, and cavity by the isosurface of liquid volumetric fraction f_L. In these figures, characteristic vortical structure of mixing layer is reproduced: primary roll-cell vortices (Kelvin-Helmholtz roller) followed by secondary streamwise vortices. Secondary vortices are stretched in the streamwise direction. This vortical structure is consistent with those in the previous experimental observations and theoretical studies of mixing layer. Cavity region is corresponding to the low-pressure area in the core of roll-cell vortices, and also in the core of streamwise vortices.

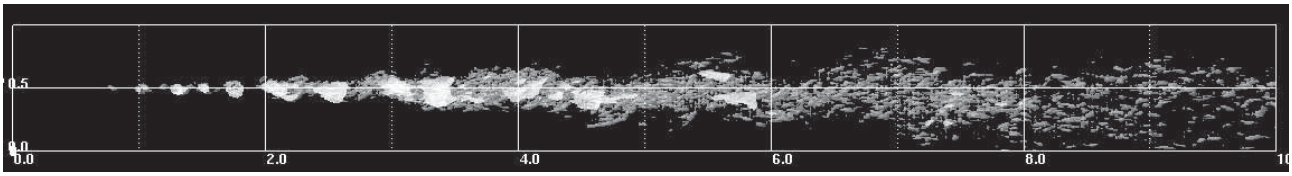

(a) Front view

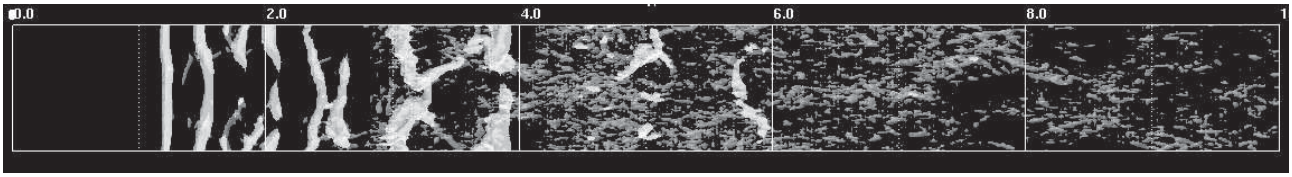

(b) Top view

Figure 2: Instantaneous contours of vortices and cavitation indicated by $Q = 230$ isosurface (gray) and isosurface of $f_L = 0.999$ (white).

TURBULENT MODULATION BY CAVITATION

Here, we analyze these DNS database under cavitating and non-cavitating conditions to investigate the interaction between cavitation and turbulence. Now we take a closer look at two different cross-section in the flow field: $x/H = 2$ and 6, respectively. Cross-section $x/H = 2$ represents the braid region, where streamwise vortices are stretched between two K-H rollers. Cross-section $x/H = 6$, on the other hand, represents the region where turbulence are fully developed and cavity generated in the upstream region collapses one after another. In the following sections, we discuss the modulation of turbulence intensity at these two different cross-sections.

Decreasing of Turbulence Intensity (Upstream region)

Figure 4 represents the distributions of normal components of Reynolds stress R_{ii} (turbulence intensity) and shear component R_{12} along y-direction in the cross-section $x/H = 2$. Hereafter, each Reynolds stress component is based on Favre average considered the fluctuation of liquid volumetric fraction f_L. Figure 3 (a) shows the time evolution of cavity area passing through this cross-section. In this cross-section, low-pressure areas in streamwise vortices are developed, so cavity mainly occurs corresponding to the streamwise vortices. At the shear layer, R_{22} and R_{33} decrease in comparison with single-phase flow. Suppressed pressure fluctuation and modulation of vortices decrease Reynolds stress.

Suppressed Pressure Fluctuation. Pressure is kept at saturated vapor pressure in cavitating region, so pressure fluctuation is less than that of single-phase flow. Under the cavitating condition, therefore, energy redistribution from R_{11} to R_{22} and R_{33} by pressure fluctuation is suppressed.

To confirm previous-mentioned effect, we focus on the pressure-strain correlation term. Figure 6 represents distribution of diagonal components of pressure-strain correlation term Π_{ii} at $x/H = 2$. In these figures, negative value means distribution 'to' other components, and positive value means distribution 'from' other components. Π_{11} and Π_{22} decrease compared with single phase. Decreasing of Π_{22} relates to decreasing of R_{22}. On the other hand, R_{11} remain almost invariant while Π_{11} increases towards positive side. When Π_{11} decreases, R_{11} is also to decrease. On the other hand, when R_{22} decreases, shear component R_{12} also decreases

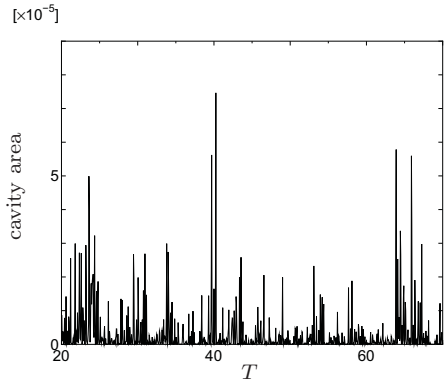

(a) $x/H = 2$

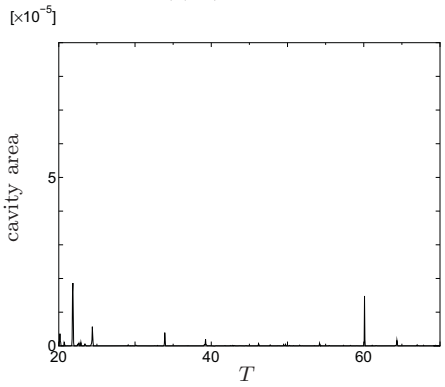

(b) $x/H = 6$

Figure 3: Time evolution of cavity area.

through production term $P_{12} = -R_{22}\partial\tilde{u}/\partial y$. Then R_{11} decreases through production term $P_{11} = -2R_{12}\partial\tilde{u}/\partial y$ when R_{12} decreases (figure 4(d)). R_{11} remains almost invariant because these two effects are balanced.

Suppressed energy redistribution by less pressure fluctuation can explain the shift of R_{11} and R_{22}, but shift of R_{33} can't be explained by this viewpoint because there is no difference of Π_{33} between cavitating and non-cavitating conditions.

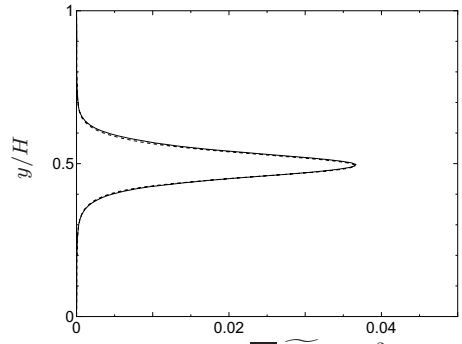

$R_{11} = \overline{f_L}\widetilde{u''u''}/\Delta U^2$

(a) R_{11}

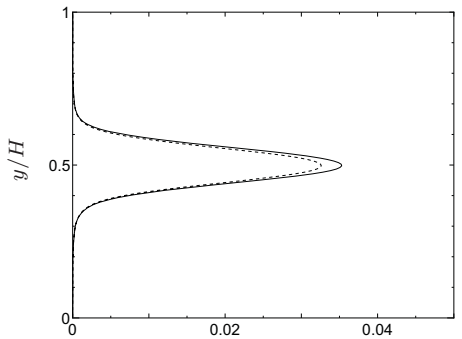

$R_{22} = \overline{f_L}\widetilde{v''v''}/\Delta U^2$

(b) R_{22}

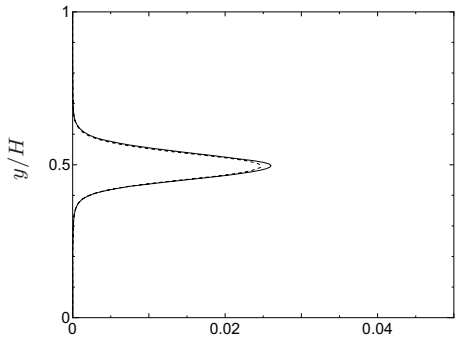

$R_{33} = \overline{f_L}\widetilde{w''w''}/\Delta U^2$

(c) R_{33}

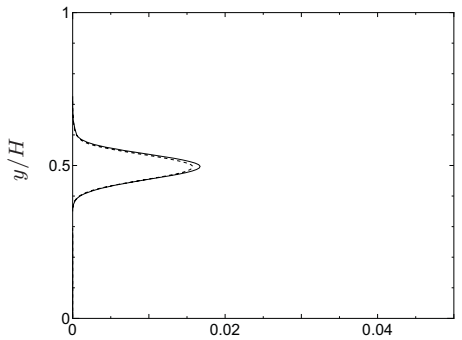

$R_{12} = \overline{f_L}\widetilde{u''v''}/\Delta U^2$

(d) R_{12}

Figure 4: Modification of Reynolds stress profiles by the cavitation at $x/H = 2$ (Solid line: single phase flow, dotted line: cavitating flow).

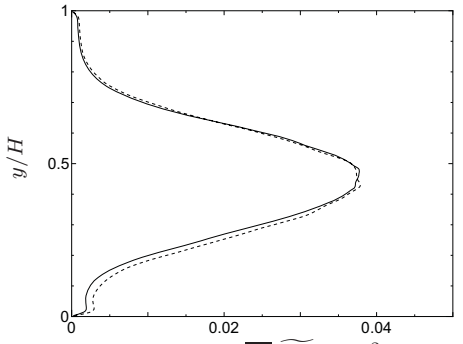

$R_{11} = \overline{f_L}\widetilde{u''u''}/\Delta U^2$

(a) R_{11}

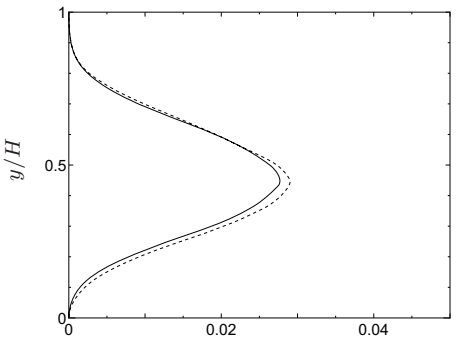

$R_{22} = \overline{f_L}\widetilde{v''v''}/\Delta U^2$

(b) R_{22}

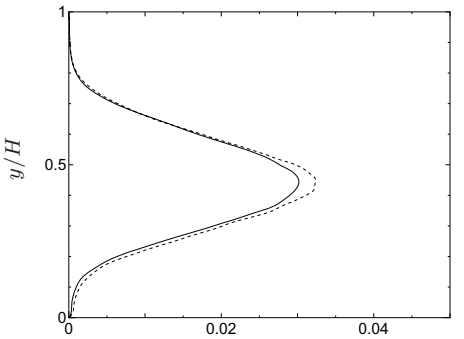

$R_{33} = \overline{f_L}\widetilde{w''w''}/\Delta U^2$

(c) R_{33}

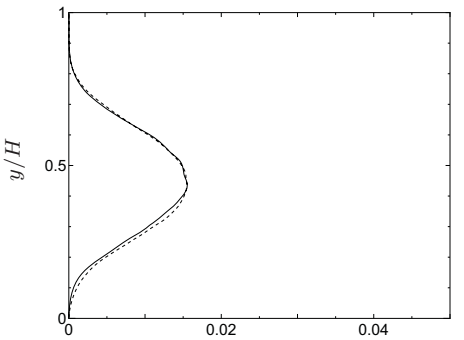

$R_{12} = \overline{f_L}\widetilde{u''v''}/\Delta U^2$

(d) R_{12}

Figure 5: Modification of Reynolds stress profiles by the cavitation at $x/H = 6$ (Solid line: single phase flow, dotted line: cavitating flow).

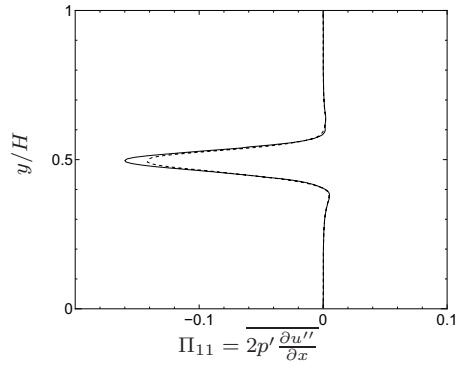

(a) Π_{11}

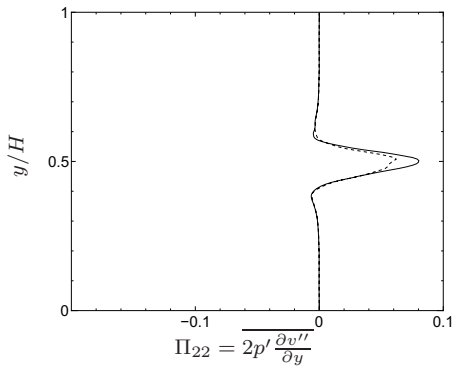

(b) Π_{22}

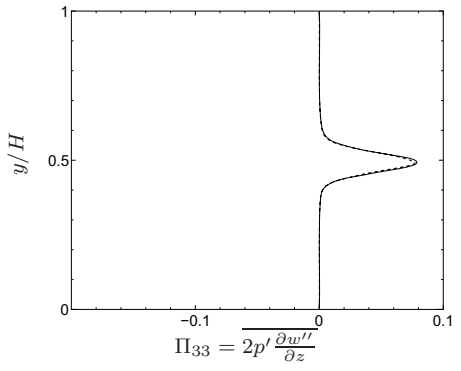

(c) Π_{33}

Figure 6: Modification of Pressure-strain correlation term by the cavitation at $x/H = 2$ (Solid line: single phase flow, dotted line: cavitating flow).

Modulation of Vortices. In this section, decreasing of R_{ii} is explained from the viewpoint of modulation of vortices.

(a) *Stretching effect*: Iyer and Ceccio (2002) considered the distribution shift of R_{22} and R_{33} based on the experiment by Belahadji et al. (1995): When streamwise vortices are stretched between two roll-cell vortices in non-cavitating conditions, circumferential velocity of vortices increase due to conservation of angular momentum, and pressure in the core decreases. As for cavitating streamwise vortices, on the other hand, stretching results only in the production of more core vapor with little change of vortex diameter, so circumferential velocity doesn't increase compared with non-cavitating vortices.

(b) *Weakened vortex by cavity expansion*: When cavity expands in a vortex, the vortex is weakened. In our previous study, we conducted a DNS of cavitation in a single vortex, and confirmed that circumferential velocity and vorticity of the vortex is decreased by cavity expansion (Kajishima et al, 2007). This interaction phenomenon between cavity and vortex is represented by a simple model, which is based on the assumption of constant circulation due to sudden cavity expansion (Kajishima et al., 2007).

These points of view, (a) and (b), can explain decrease of R_{22} and R_{33} shown in figure 4: circumferential velocity of streamwise vortices corresponds to components of R_{22} and R_{33}. As for (b), K-H rollers are also weakened by cavity expansion, so R_{11} and R_{22} decrease in the region where cavity occurs in roll-cell vortices (figure omitted).

Increasing of Turbulence Intensity (Downstream region)

In the downstream region, on the other hand, turbulence intensity tends to increase in comparison with single-phase flow. Figure 5 represents the distributions of normal and shear components of Reynolds stress in the cross-section $x/H = 6$. In figure 5, three normal components tend to increase in comparison with single-phase flow. Figure 3 (b) shows the time evolution of cavity area passing through this cross-section. Cavity generated in the upstream region collapses one after another in this region. Collapse of cavity causes fluctuation of velocity. That's why the turbulence intensity are insreased in the downstream region.

CONCLUSION

The interaction between cavitation and turbulence is investigated by DNS. The DNS results suggest that turbulence intensity decreased in actively cavitating region compared with non-cavitating condition. This decreasing is explained by suppressed energy redistribution by less pressure fluctuation and vortex modification. In the region where cavity collapsing is dominant rather than cavity generating, turbulence intensity tends to increase.

In this computation, we could observe that a typical free turbulence is modulated by cavitation. We will propose a cavitation LES model which is based on One-equation dynamic model (Kajishima & Nomachi, 2003). In One-equation dynamic model, turbulent energy K_{SGS} transport equation is dealt with to obtain the eddy-viscosity dynamically. This enables us to introduce the cavitation effect to the SGS flow field as the source term of K_{SGS} transport equation. We must consider two-way interaction when formulating the source term: namely, the prediction of cavitation inception due to the SGS vortices and the source of turbulence energy due to the cavitation. In the present study, the latter part is particularly highlighted. The flow around the cavitating vortex has been captured by our former work (Kajishima et al., 2007) and it is used for the extra term in K_{SGS} equation. Then this concept will be evaluated in a priori manner by filtering the DNS database.

REFERENCES

Arndt, R. E. A., 2002, "Cavitation in Vortical Flows," *Annu. Rev. Fluid Mech.*, Vol. 34, pp. 143-175.

Belahadji, B. et al., 1995, "Cavitation in the Rotational Structures of a Turbulent Wake," *J. Fluid Mech.*, Vol. 287, pp. 383-403.

Chen, Y., and Heister, S., 1995, "Two-phase Modeling of Cavitated Flows," *Computer & Fluids*, Vol. 24-7, pp. 799-809.

Coutier-Delgosha, O. et al., 2003, "Numerical Simulation

of the Unsteady Behaviour of Cavitating Flows," *Int. J. Numer. Meth. Fluids*, Vol. 42, pp. 527-548.

Inagaki, M. et al., 2000, "Numerical Prediction of Fluid-Resonant Oscillations at Low Mach Number," *Trans. of the Japan Society of Mech. Eng. Series B*, Vol. 66-649, pp,2274-2281 (in Japanese).

Iyer, C. O. and Ceccio, S. L., 2002, "The Influence of Developed Cavitation on the Flow of a Turbulent Shear Llayer," *Phys. of Fluids*, Vol. 14-10, pp. 3414-3431.

Kajishima, T. and Nomachi, T., 2003, "One-equation Subgrid Scale Model Using Dynamic Procedure for the Energy Production," *ASME FEDSM2003*, CD-ROM, No. 45348.

Kajishima, T., Ohta, T., Sakai, H. and Okabayashi, K., 2007, "Influence of Cavitation on Turbulent Separated Flow," *Proc. 5th International Symposium on Turbulence and Shear Flow Phenomena (TSFP5)*, CD-ROM.

Kunz, R. F. et al., 2000, "A Preconditioned Navier-Stokes Method for Two-phase Flows with Application to Cavitation Prediction, " *Computer & Fluids*, Vol. 29, pp. 849-875.

Okita, K. and Kajishima, T., 2002, "Three-dimensional Computation of Unsteady Cavitating Flow in a Cascade," *Proc. 9th International Symposium on Transport Phenomena and Dynamic of Rotating Machinery*, CD-ROM, No.FD-ABS-076.

Senocak, I. and Shyy, W., 2002, "A Pressure-based Method for Turbulent Cavitating Flow Computations," *J. Comp. Phys.*, Vol. 176, pp. 363-383.

Ugajin, H. et al., 2006, "Numerical Simulation of Unsteady Cavitating Flow in a Turbopump Inducer," *Proc. of 42nd AIAA/ASME/SAE/ASEE Joint Propulsion Conference*, CD-ROM, AIAA2006-5068.

Wang, G. and Ostoja-Starzewski, M., 2007, "Large Eddy Simulation of a Sheet/cloud Cavitaiton on a NACA0015 Hydrofoil," *Appl. Mathematical Modeling*, Vol. 31-3, pp. 417-447.

Wienken, W. et al., 2006, "A Method to Predict Cavitation Inception Using Large-Eddy Simulation and Its Application to the Flow past a Square Cylinder," *J. Fluids Eng.*, Vol. 128-2, pp. 316-325.

Yamanishi, N. et al., 2007, "LES Simulation of Backflow Vortex Structure at the Inlet of an Inducer," *Trans. of the ASME, J. Fluids Eng.*, Vol. 129-5, pp. 587-594.